Combined Experimental and Theoretical Approach to the Study of Structure and Dynamics of the Most Inert Aqua Ion [Ir(H₂O)₆]³⁺ in Aqueous Solution

Flora Carrera,[†] **Francisco Torrico,**[‡] **David T. Richens,**[§] **Adela Muñoz-Páez,**[†] **José M. Martínez,**[‡] **Rafael R. Pappalardo,**[‡] **and Enrique Sánchez Marcos*,**[‡]

Departamento de Química Inorgánica, ICMSE, CSIC, Universidad de Sevilla, 41012 Sevilla, Spain, Departamento de Química Física, Universidad de Sevilla, 41012 Sevilla, Spain, and School of Chemistry, University of St. Andrews, Purdie Building, St. Andrews, Fife KY16 9ST, United Kingdom

Quantitative determination of the hydration structure of hexaaquairidium(III), $[Ir(H_2O)_6]^{3+}$, in aqueous solution, the most inert aqua ion known, has been achieved for the first time by a combined experimental−theoretical approach employing X-ray absorption spectroscopy and molecular dynamics (MD) simulations. The Ir L_{III}-edge extended X-ray absorption fine structure (EXAFS) spectrum and L_I-, L_{II}-, and L_{III}-edge X-ray absorption near-edge structure (XANES) spectra of three concentrations of $[Ir(H_2O)_6]^{3+}$ in perchloric acid media were measured. To carry out classical MD simulations of the aqua ion in water, a new set of first-principles Ir−H_2O intermolecular potentials, based on the hydrated ion concept, has been developed. Structural, dynamics, and energetic properties have been obtained from the analysis of the statistical trajectories generated. The Ir−O radial distribution function shows two well-defined peaks at 2.04 ± 0.01 and 4.05 ± 0.05 Å corresponding to the first and second hydration shell, respectively; the fundamental frequencies for the aqua ion in water are well reproduced by the MD simulation, and its dynamic properties are similar to the experimental values corresponding to other hexahydrated trivalent ions. Particular attention has been devoted to the experimental determination of the second hydration shell. It has been found that contrarily to what expected on the basis of the inertness of the Ir³⁺ aquaion, the detection of the second hydration shell by EXAFS for this cation is more difficult than for others less inert aqua ions such as Cr³⁺ or Rh³⁺. But when combined with MD simulations it is possible to confirm the coordination distance for this shell at 4.1 ± 0.1 Å. In addition, the computation of L_I, L_{II} and L_{III} XANES spectra were carried out using the structural information obtained from MD. These computations allowed the assignment of special features of the spectra to the second hydration shell on a quantitative basis. Therefore, interestingly XANES spectra have given a stronger support to the second hydration shell than EXAFS. The fit of the L_{III}-edge EXAFS gives an accurate description of the first hydration shell structure in aqueous solution. The value for Ir−O first shell is 2.04 ± 0.01 Å. The statistical information available with the MD results has allowed the analysis of the standard deviation associated with the computation of the XANES spectrum. It is shown that the standard deviation increases with the number of hydration shells and this increase is nonuniform along the average spectrum.

Introduction

Structural and dynamic properties of metal ions in aqueous solution have long been a classical topic in solution chemistry due to their huge number of applications in chemistry, physics, biology, earth sciences, and engineering.[1−4] There is abundant structural information available for the stable aqua ions, $[M(H_2O)_n]^{m+}$, in aqueous solutions, usually obtained with the aid of diffraction or spectroscopic techniques.[5−7] Aqueous solutions of metal aqua ions represent an ideal benchmark to check the capabilities of a given technique to investigate the detection limit around the ion, such as how accurately and how far from the metal ion could be characterized and which are the measurable upper and lower concentration limits, etc. The possible experimental and theoretical technical refinements for the structural elucidation that could be achieved in these benchmark studies might be applied to the characterization of ion environments in more complex systems. In these cases,

where in general the metal ion concentration is low, the possibility of analyzing the structure beyond the closest environment, that is, the first coordination shell of atoms, is of relevance for identification and location purposes, such as the coordination mode of a given ligand, anchoring region of a metal cation in biomolecules or confined systems, etc.

One of the techniques better suited to obtain such information is X-ray absorption spectroscopy (XAS); since it is element-specific, it can be applied to the study of species in either the solid, liquid, or gas state, it is sensitive to short-range order, and it can provide information about low concentration species. The study of the hydration structure of highly diluted cationic species is especially useful for acquiring information concerning cation−water interactions nonperturbed by ion−ion interactions. XAS spectra are usually split into two regions, the X-ray absorption near-edge structure (XANES) part, which involves a region of 100 eV around the edge energy, and the extended X-ray absorption fine structure (EXAFS) part, which extends from ca. 60 eV up to 1000 eV above the edge. Sayers et al.[8] have proposed an EXAFS equation that allows the determination of the coordination number and distances as well as the type of coordinating atoms around the absorber ion. Moreover the mean

---

* Author to whom correspondence should be addressed. E-mail: sanchez@us.es.
† Departamento de Química Inorgánica, Universidad de Sevilla.
‡ Departamento de Química Física, Universidad de Sevilla.
§ University of St. Andrews.

standard deviation for coordination distance provides information about static and dynamic disorder and thus, indirectly in some special cases, about the kinetic stability of species in solution.[9] The main limitation of the technique is the high correlation among factors affecting the amplitude, i.e., coordination number and the Debye−Waller (DW) factor, which accounts for static and dynamic disorder.[10]

A strategy to reduce the degree of uncertainty in the analysis of the XAS spectra has been the inclusion of independent information derived from computer simulations.[11−16] Provided that reliable structural and dynamic information is obtained from computer simulations, the microscopic description of the close environment of the absorber atom is relevant in twofold. On one hand, it allows the independent computation of some of the parameters involved in the spectroscopic data analysis; on the other hand, it allows the assignment of certain features of a given spectrum to particular structural arrangements around the ion.

A primary requirement for expecting a well-defined hydration structure in an aqua ion is high stability coupled with high inertness. In a pioneering report on the solvent exchange kinetics, Hunt and Taube[17] established that hexaaquachromium-(III), $[Cr(H_2O)_6]^{3+}$, exhibits an extremely slow rate of exchange (lifetimes of a first-shell water molecule at 298 K on the order of 4 days). $[Rh(H_2O)_6]^{3+}$ was later shown to be even more inert (lifetimes of ca. 12 years).[18] On this basis $[Ir(H_2O)_6]^{3+}$ was therefore expected to show an even higher degree of inertness toward water exchange. Although $[Ir(H_2O)_6]^{3+}$ was prepared for the first time in 1976 by Beutler and Gamsjäger[19] and its coordination number in solution was later verified by the same workers in 1978 using an ^{18}O-tracer technique,[20] detailed knowledge of solution dynamics only became apparent 20 years later when Cusanelli et al.[21] developed high-temperature and high-pressure ^{17}O NMR kinetic equipment enabling quantitative measurement of the rate of the water exchange process. The quantitative results confirmed the high degree of inertness of $[Ir(H_2O)_6]^{3+}$, $k_{exch}^{298K} = 1.1 \times 10^{-10}$ s^{-1}, implying a mean lifetime for the first-shell water molecules at 298 K of ∼300 years. For this reason very few water ligand complexation reactions within the primary shell have been successfully studied.[22,23] Paradoxically, although the aqua ion is very inert, it is difficult to synthesize the monomeric species of this aqua ion due to its facility to polymerize. This has strongly limited the measurements of experimental data in aqueous solution.

The combination of the extremely high stability and inertness of its first hydration shell, its high charge, and its octahedral structure make the Ir(III) aqua ion a paradigm of the hydrated ion concept that promotes a concentric shells hydration structure, as proposed by Frank and Evans.[24] Within this model the existence of a well-defined second hydration shell must be expected. Use of low concentrations of Ir(III) are important to minimize ion−ion interactions such that under these conditions XAS is the most appropriate technique. Structural parameters for the Ir−O distance in a related solid compound containing the hexaaqua motif have been obtained by means of X-ray diffraction for the crystal of the cesium sulfate alum CsIr(SO$_4$)$_2$·12H$_2$O, being determined a value of 2.04 Å.[25] In the present work, XAFS measurements of the Ir(III) aqua ion in aqueous solution have been carried out by recording the three Ir L-edge absorption spectra, and both the EXAFS and the XANES regions of the XAS spectrum have been analyzed. We have already shown for the cases of $[Cr(H_2O)_6]^{3+}$ and $[Rh(H_2O)_6]^{3+}$ that EXAFS[26,27] and XANES[28] are capable of detecting the second hydration shell. The power of the combined analysis is illustrated

by the recent work of D'Angelo et al.,[29] who have succeeded in detecting the presence of the second hydration shell in the case of $[Ni(H_2O)_6]^{2+}$ following a quite similar XANES/molecular dynamics (MD) approach to that proposed by us in previous work[28] while reaching similar conclusions.

The information thus obtained from an experimental source has been complemented with theoretical results derived from MD simulations of Ir(III) in water. To this purpose a new intermolecular potential for iridium−water, based on the hydrated ion concept developed by our group has been built.[30−32] The key point of this strategy is to recognize that water molecules belonging to the first hydration shell are so strongly perturbed by the presence of the highly charged metal ion that they might be treated differently from the bulk water molecules. From the concentric shell model proposed by Frank and Evans,[24] this distinction among water molecules can be implemented by defining in the simulated solution two types of solvent molecules: those forming the first shell, inside a spherical shell surrounding the cation, and the bulk solvent molecules characterizing the solvent properties. Within this framework, the primary requirement of the model is that the two types of water molecules remain within their regions during the simulation. In other words, the hydrated ion concept is strictly applicable to those metal cations where the rate constant of the first shell water exchange is slow, i.e., residence lifetimes higher than a few tens of nanoseconds. In this respect, the extremely slow water exchange rate for $[Ir(H_2O)_6]^{3+}$ [19] means that it should prove to be the best example yet for applying our statistical implementation of the hydrated ion concept.

The aim of this work is to present the structural results derived from experimental and theoretical methods and from a combination of them. Particular attention is devoted to the experimental determination of the second hydration shell. Thus, on one hand, the EXAFS and XANES analysis for the Ir(III) aqua ion water solutions explore the detection limit of the techniques adopting the usual experimental tools; on the other hand the structural and dynamical results obtained from the MD simulations of an aqueous solution of the same aqua ion provide the theoretical view. Finally, the synergy achieved by combining both spectroscopic and theoretical results improves the analysis process in two ways: (i) by refining the XAS data analysis and (ii) by supporting the intermolecular potential developed as well as the microscopic vision of the hydration derived from computer simulations.

Experimental Section

Preparation of Solutions of $[Ir(H_2O)_6]^{3+}$ in 2.0 M HClO$_4$. The synthesis described is an adaption[12] of that originally reported by Beutler and Gamsjager.[19] Na$_2$[IrCl$_6$]·6H$_2$O (2.0 g, 3.6 mmol) was treated with a deoxygenated solution of 0.2 M sodium hydroxide (1000 cm^3) at 40 °C for ca. 5 h. After 2 h, ascorbic acid (0.2 g) was added to the stirred iridium solution to prevent atmospheric oxidation. Adjustment of the solution to pH 6 by the dropwise addition of 2.0 M HClO$_4$ then gave a cream precipitate of active iridium(III) hydroxide hydrate $[Ir(H_2O)_3(OH)_3]$. The precipitate was then separated by centrifugation and washed with double-distilled water (2 × 100 cm^3). After dissolution of the precipitate in 0.1 M HClO$_4$ the resulting yellow solution was loaded onto a Dowex 50W-X2 200−400 mesh cation exchange column (10 cm × 1 cm). Elution with 2.0 M HClO$_4$ afforded solutions of 20-50 mM $[Ir(H_2O)_6]^{3+}$ in a total overall yield of 34% as checked by UV/vis absorption spectroscopy (λ_{max} 262 nm, ($\epsilon = 36.6$), and 311 ($\epsilon = 30.8$)).[21,33] This procedure was repeated until a total of 10 g of Na$_2$[IrCl$_6$]·

Structure and Dynamics of [Ir(H$_2$O)$_6$]$^{3+}$

J. Phys. Chem. B, Vol. 111, No. 28, 2007 **8225**

6H$_2$O had been converted to solutions of the aqua ion. Three solutions containing 0.05, 0.15, and 0.33 M [Ir(H$_2$O)$_6$]$^{3+}$ in 2−3 M HClO$_4$ were obtained by solvent evaporation under low pressure.

X-ray Absorption Measurements and Data Analysis. XAS spectra of the three Ir L-edges (E = 13 419, 12 824, and 11215 eV for L$_I$, L$_{II}$, and L$_{III}$, respectively) of the 0.33, 0.15, and 0.05 M solutions of [Ir(H$_2$O)$_6$]$^{3+}$ were carried out at the synchrotron radiation source ESRF, in Grenoble, France, at station BM29. The ring energy was 6 GeV, and the ring current was 200 mA. Energy calibration was carried with a Pt foil, showing an L$_{III}$ edge at 11 564 eV. A double-crystal Si(311) monochromator was used. Higher harmonic rejection was carried out by detuning both crystals 50%. Measurements were carried out at room temperature in transmission detection mode, using the ionization chamber as detectors. The XANES region of the XAS spectrum for the Ir L$_I$- and L$_{II}$-edges for the three solutions were obtained by scanning 300 eV around the edges and the EXAFS and XANES spectra of the L$_{III}$ edge, the most intense one by scanning 1000 eV around it.

Standard methods were used to perform background subtraction, E_0 determination, and normalization, as explained elsewhere.[26] Single and multiple scattering (SS, MS) contributions were taken into account to perform the fit of the EXAFS data. To reduce the number of free parameters, those required for the MS paths were derived from the corresponding SS paths: multiplying coordination distances by the appropriate factor and applying the relationships of the independent vibration model[34] to obtain DW factors. This approach has proven to be accurate for similar analysis on the [Cr(H$_2$O)$_6$]$^{3+}$ and [Rh(H$_2$O)$_6$]$^{3+}$ aqua ions as deduced from combined EXAFS and MD calculations.[28]

With the selected model structures, computation of the relevant paths were carried out with the FEFF program developed by Rehr[35] (version 8.10), taking into account the restrictions concerning path lengths (R > 5Å) and amplitudes (>5% of that of the most intense path) described elsewhere.[26] The relevant contributions, thus obtained with FEFF, were computed with the aid of FEFFIT code (version 2.98)[36] to fit the experimental spectra.

Theoretical Calculations

Ion−Water Interaction Potentials. The ion−water interaction potentials developed for Ir(III) are based on the flexible hydrated ion model[32] previously applied to several highly charged metal ions and described in detail elsewhere.[37−39] Briefly, in this model, the interactions of the metal ion in aqueous solutions are described by two intermolecular potentials obtained from ab initio calculations. The first one called HIW[30,31] accounts for the hydrated ion−bulk solvent interactions and adopts a site−site form involving the following expression

$$E_{HIW} = \sum_i^{HI\ sites} \sum_j^{W\ sites} \frac{A_4^{ij}}{r_{ij}^4} + \frac{A_6^{ij}}{r_{ij}^6} + \frac{A_{12}^{ij}}{r_{ij}^{12}} + \frac{q_i q_j}{r_{ij}}$$

while the internal dynamics of the first hydration shell is defined through the IW1 potential that accounts for the cation−first shell water molecules interactions (O$_I$ denotes an oxygen atom of the water molecules in the first shell)

$$E_{IW1} = \frac{B_4^{IrO_I}}{r_{IrO_I}^4} + \frac{B_6^{IrO_I}}{r_{IrO_I}^6} + \frac{B_7^{IrO_I}}{r_{IrO_I}^7} + \frac{B_{12}^{IrO_I}}{r_{IrO_I}^{12}} + \sum_i^{W_I\ sites} \frac{q_{Ir} q_i}{r_{ij}}$$

and the chosen intermolecular potential to describe the interactions among the water molecules. In this case, the TIP4P[40] intermolecular potential was used for describing the water solvent, although there is not any restriction to choose another water model interaction potential.

The observed degree of transferability in the HIW potential among different divalent and trivalent cations[37] allows us to use the A coefficients obtained from Cr(III).[32] However, the B IW1 coefficients are cation-specific, so they must be developed for each case. Electrostatic charges appearing in both HIW and IW1 expressions also are specific for each hydrated ion and have been obtained by fitting a set of atomic charges that reproduce the electrostatic potential generated by the wavefunction of the hydrated ion, [Ir(H$_2$O)$_6$]$^{3+}$, in this case.

The reference structure for the iridium aquaion is obtained by an optimization at the MP2 level, using the Stuttgart/Dresden relativistic effective core potential[41] for the Ir atom. The SDD basis sets were used for the Ir atom, and correlation-consistent polarized valence basis sets of double-ζ quality augmented by diffuse functions (aug-cc-pvdz) were used for the O and H atoms.[42] At this level, the optimized geometrical parameters of the hydrate (T_h symmetry) are: R_{Ir-O} = 2.056 Å, R_{O-H} = 0.976 Å, and ∠HOH = 109.4°.
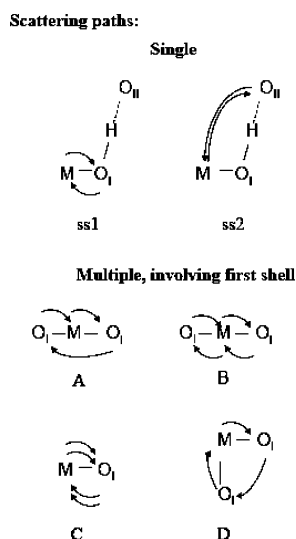
To include solvent effects on the set of effective atomic charges employed in the HIW and IW1 expressions, the hydrate wavefunction is polarized by means of the polarizable continuum model[43] developed at Pisa. CHELPG[44] charges are then obtained from the polarized wavefunction.

The IW1 building implies the fitting of a set of interaction energies inside the hydrate corresponding to geometrical deformations from the reference (T_h) structure, ca. 60 distorted structures were considered. The final set of IW1 parameters and electrostatic charges used in the molecular dynamics simulations are: q_{Ir} = 1.9332, q_{O_I} = −1.0022, q_{H_I} = 0.5900, $B_4^{IrO_I}$ = −9680.91, $B_6^{IrO_I}$ = 82274.19, $B_7^{IrO_I}$ = −100142.02, $B_{12}^{IrO_I}$ = 99619.47 (coefficients given in kcal Å^n/mol and charges in fractions of e).

Molecular Dynamics Simulation Details. A molecular dynamics simulation of a system composed of one Ir(III) ion plus 500 water molecules, six of these forming the hydrate, (H$_2$O)$_I$, (density = 0.997 g/cm^3) was performed in the canonical ensemble (NVT) at 298 K using periodic boundary conditions. The Nosé−Hoover thermostat approach[45] was employed to control the temperature. Simulation was performed using Moldy code[46] that employs a symplectic algorithm of the leapfrog type following the quaternion formalism for rigid bodies. A time step of 2 fs was used, and a cut-off distance of 12 Å was applied for the short-range terms. The Ewald sum methodology[47] was applied to account for the electrostatic interactions, including the charged system term.[48,49] Simulations with net charged cells can be performed using an energy correction term that is physically equivalent to adding a uniform jelly of charge that exactly neutralizes the total cell charge.[50] Although more sophisticated corrections have been proposed,[51] these concern simulations in which the volume, the system shape, or the net charge is altered during the simulation process. The production period was extended for 1 ns, saving trajectories every 20 fs for further analysis.

EXAFS Spectrum Computations. From the trajectory computed by the MD simulation, a set of 1000 snapshots evenly spaced were taken for the simulation of the EXAFS part. As presented in previous works,[28b,52] the EXAFS function is obtained by averaging the individual $\chi_s(k)$ computed for each snapshot. Then, the disorder arises from the nonsymmetric

SCHEME 1:   Main Scattering Paths Contributing to the EXAFS Spectrum: First and Second Hydration Shell Single Scattering and First-Shell Multiple Scattering at the Oxygen Sites
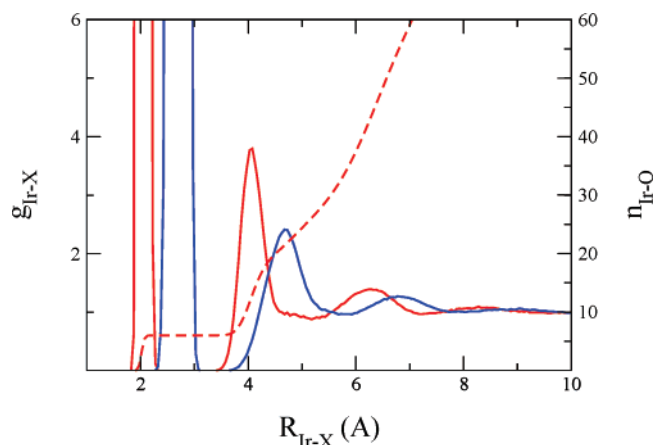

Figure 1. Iridium−oxygen (red) and iridium−hydrogen (blue) radial distribution functions derived from MD simulation and running integration number for Ir−O (red dashed line).

arrangement of each snaphsot and from summing over the representative number of MD structural arrangements. This procedure differs from the classical EXAFS equation[8] since the Debye−Waller factors are excluded from the expression employed to compute the simulated EXAFS function and a new sum over N_s structures (MD snapshots) appears

$$\chi(k) = \frac{1}{N_s} \sum_s^{N_s} \chi_s(k) =$$

$$\frac{1}{N_s} \sum_s^{N_s} \sum_j^{\text{paths}} \frac{N_j S_o^2}{kR_{sj}^2} |f^{\text{eff}}(k,R)| \sin(2kR_{sj} + \varphi_j(k)) \, e^{-2R_{sj}/\lambda} \quad (1)$$

where s goes over the structures obtained from the statistical sampling, and j goes over all the paths generated from each structure, restricted to a maximum path-length of 5 Å and 4 legs. Typically, ca. 80 paths are included when $R_{\text{cutoff}} = 6$ Å and 30 paths when $R_{\text{cutoff}} = 3.1$ Å. Scheme 1 plots the most significant types of paths generated.

Two simulated EXAFS spectra were computed. The first one was computed considering all of the atoms within a sphere around the central cation of 6 Å ($R_{\text{cutoff}} = 6$ Å); according to the radial distribution functions (RDFs), this sphere encloses completely the oxygen and hydrogen atoms of the first and second hydration shells. Tests using longer R_{cutoff} values did not change the EXAFS function. The second simulated spectrum was computed using $R_{\text{cutoff}} = 3.1$ Å, according to the Ir−O and Ir−H RDFs (Figure 1) this cut-off radius encloses only the water molecules belonging to the first hydration shell. XAS calculations were performed with the FEFF program (version 8.10).[35] The subsequent application of FEFFIT code (version 2.98)[36] yielded the spectra in *r*-space and the corresponding fitting of the simulated spectra.

The values employed in the EXAFS spectra, for the amplitude reduction factor, S_o^2 (0.87), and the inner potential correction, ΔE_o (14.8 eV), were those obtained by fitting the experimental EXAFS spectrum given in Table 2. For technical details, one of the input FEFF file used for a given snapshot is given as Supporting Information .

XANES Spectrum Computations. L_I-, L_{II}-, and L_{III}-edge XANES spectra of $[Ir(H_2O)_6]^{3+}$ in water were calculated using

TABLE 1: Molecular Dynamics Results[a]

	structure[b]			
	R_I^{max} (Å)	N_I	R_{II}^{max} (Å)	N_{II}
g_{Ir-O}	2.04 (2.041)[25]	6	4.05	14−15
g_{Ir-H}	2.72	12	4.65	
	energetics			
$\Delta H_{\text{hydr}}(Ir(III))$ (kcal/mol)	−1314 ± 40			
	dynamics[c]			
$D_{Ir^{3+}}(10^{-5}\, cm^2\, s^{-1})$	0.6 ± 0.1			
	$t^* = 0$ ps		$t^* = 2$ ps	
$\tau_{\text{MRT}}^{\text{2nd shell}}$	9 ± 1		19 ± 1	
	normal modes[d]			
A_g (cm^{-1})	595 ± 5 (554)[53]			
E_g (cm^{-1})	510 ± 5 (540)[53]			
T_u (cm^{-1})	565 ± 5 (490)[53]			

[a] Values in parenthesis correspond to experimental estimations, and superscripts indicate the reference where they can be found. [b] RDF maxima and running integration numbers for first and second hydration shells. [c] Ion diffusion coefficient and mean residence times for water molecules in the second hydration shell. [d] Fundamental M−O stretching modes (see ref 53 for definition).

TABLE 2: Parameters Obtained for the First and Second Hydration Shell from the Fit of the EXAFS Spectrum of $[Ir(H_2O)_6]^{3+}$ and from the MD Simulation

	EXAFS fitting[a]		MD results[b]	
path	R	σ^2	$\langle R \rangle$	σ^2
ss1	2.04 ± 0.01	0.0022 ± 0.001	2.04 ± 0.04	0.0018 ± 0.0005
ss2	4.05 ± 0.10	0.06 ± 0.01	4.14 ± 0.08	0.054 ± 0.005
A	4.07	0.004	4.09	0.0033
B	4.07	0.004	4.09	0.0034
C	4.07	0.009	4.09	0.0071
D	3.48	0.006	3.49	0.0050

[a] Goodness of fit value, $\mathscr{R} = 0.015$, Δk (Å^{-1}) = 2.8−17; ΔR (Å) = 1.0−5.0; ΔE_0 (eV) = 14.4; $S_0^2 = 0.87$, $N_{II} = 14$. [b] $N_{II} = 14$.

the structures of 200 snapshots taken every 5 ps from the MD simulation above-described. The three simulated edges were obtained by averaging the spectra of the same set of snapshots.

The spectra were computed with the FEFF program.[35] The potential calculations use the Hedin−Lundqvist self-energy approximation, and the electron density distribution was obtained self-consistently (SCF procedure). An SCF radius centered on each type of atom was set to 6.0 Å. Two types of oxygen atoms were considered in the calculations: first-shell and bulk oxygen atoms. The strong perturbation of water molecules closer to the metal ion is then accounted for, and consequently two different
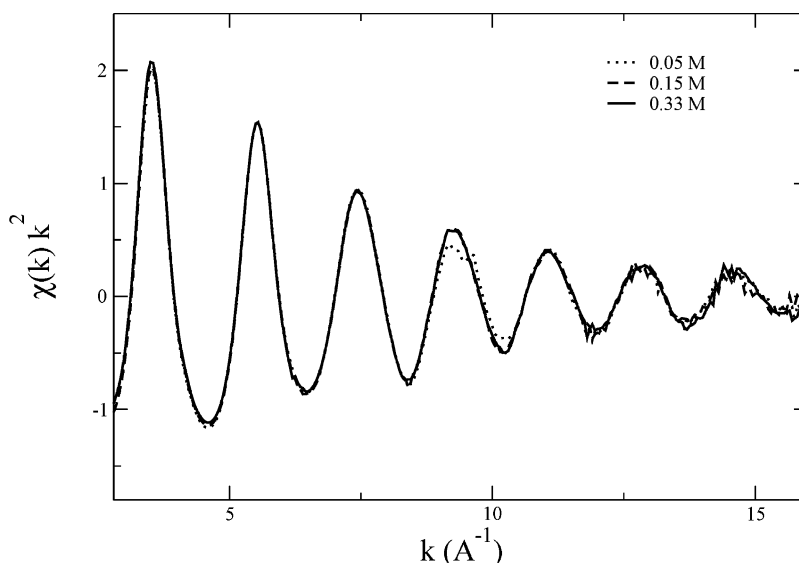
Structure and Dynamics of $[Ir(H_2O)_6]^{3+}$

J. Phys. Chem. B, Vol. 111, No. 28, 2007 **8227**

Figure 2. Experimental Ir L$_{III}$-edge EXAFS spectra for the three aqueous concentrations of the $[Ir(H_2O)_6]^{3+}$ aqua ion.

backscattering behaviors are assigned to both types of oxygen atoms. Full multiple scattering (FMS) computations were performed within a sphere of 6.0 Å around the Ir center for the XANES computation, ensuring in this way the inclusion of the second and part of the third hydration shells in the computation of the spectra. As in the previous studies on the $[Cr(H_2O)_6]^{3+}$ and $[Rh(H_2O)_6]^{3+}$ aqua ions, the hydrogen atoms were taken into account to compute the potential, but they were not included as backscatterers.[13,15] For technical details, one of the input FEFF file used is given as Supporting Information.

Results and Discussion

Molecular Dynamics Results. Radial distribution functions for the Ir—O and Ir—H pairs are shown in Figure 1. The first Ir—O peak, centered at 2.04 Å, sharply defines the first hydration sphere, while a well-defined second maximum, corresponding to the second hydration shell formed by 14—15 water molecules, is observed at 4.05 Å. Even a third maximum is present in the 6—7 Å region. A similar distribution is observed for the Ir—H RDF but with maxima positions at larger distances due to the water orientation imposed by the metal cation. These results reflect a well-defined hydration structure around the cation, as expected for a stable trivalent aquaion such as Ir(III).

Molecular dynamics simulation analysis provides not only structural information such as radial distribution functions but also energetic, dynamic, or even spectroscopic information, difficult to obtain experimentally in some cases. Details about the analysis performed to obtain the set of properties collected in Table 1 can be found elsewhere.[32,37−39]

Due to the difficulties in the synthesis of the homoleptic species, $[Ir(H_2O)_6]^{3+}$ aqua ion, very little experimental information of aqueous solutions containing it has been published so far.[23] Therefore the comparison between simulation and experimental results is very limited. In fact, no structural information is available for the liquid state, and there is only a study[25] providing structural information on the hexahydrate motif in a crystal, the above-mentioned value for the Ir—O$_I$ distance in the corresponding Ir(III) cesium sulfate alum (2.041 Å).[25] Similar values for the crystallographic distance and the MD simulation in water (2.04 ± 0.01 Å) reflect the robustness of the $[Ir(H_2O)_6]^{3+}$ entity and indicate that condensed phase effects due to crystal packing or solvent effects only introduces change in some hundredths of ångstroms. The Ir—O$_I$ distance for the

quantum-mechanical-optimized structure of $[Ir(H_2O)_6]^{3+}$, i.e., the representative structure without condensed phase medium, is 2.056 Å. The fundamental frequencies for the aqua ion in aqueous solution, in the far-infrared region, have been determined by IR and Raman spectroscopic measurements.[53] The three M—O stretching modes computed from the simulation analysis are in reasonable agreement with the experimental estimations (Table 1). The dynamic properties collected in Table 1, such as cation self-diffusion coefficient (D_{Ir}) or mean residence times of the second-shell water molecules (τ_{MRT}^{2shell}) are very similar to the values previously obtained for other hexahydrated trivalent ions such as $[Cr(H_2O)_6]^{3+}$, $[Rh(H_2O)_6]^{3+}$, or $[Al(H_2O)_6]^{3+}$.[32,37,38] Taking into account that the specificity of the metal ion is buffered by the first shell of water molecules, the results presented here seem to show the good behavior of the cation−water interaction potentials employed in this work.

L$_{III}$-Edge Ir EXAFS Spectrum of Ir(III) Aqueous Solution. Figure 2 shows the Ir L$_{III}$ EXAFS spectra of three aqueous solutions containing $[Ir(H_2O)_6]^{3+}$ complex at three different concentrations, 0.05, 0.15, and 0.33 M. As seen there, the three spectra superimpose, being the only difference the higher noise amplitude of the most diluted solution, which induces a distortion around 10 Å^{-1}. The similarity among the three spectra is of relevance since it discards the existence of polymerized species, which should show a dependence on the concentration. Polymeric species are those usually obtained when dissolving an Ir(III) salt in water. For this reason, the elaborate synthesis method described in the Experimental Section has to be followed to avoid the formation of such polymeric species. In these species, the centers of two contiguous octahedra are occupied by Ir(III) cations, which are ca. 3 Å apart. Then, if formed, the polymeric species should have the highest concentration in the most concentrated solution and should show an Ir—Ir contribution to the EXAFS signal at this distance. Since Ir is a heavy backscatterer, this contribution should be rather intense and completely different, both in phase shift and in amplitude, from that of the Ir—O contribution. The similarity among the three spectra as well as their shapes confirms that the unique species present in the three solutions are the homoleptic $[Ir(H_2O)_6]^{3+}$.

These spectra are similar to those of other di- and trivalent transition metal cations, and it can be described as a quasi-simple wave. When compared with other spectra of divalent cations, such as Zn^{2+}, Ni^{2+}, Co^{2+}, Mn^{2+}, Ca^{2+}, Pt^{2+}, or
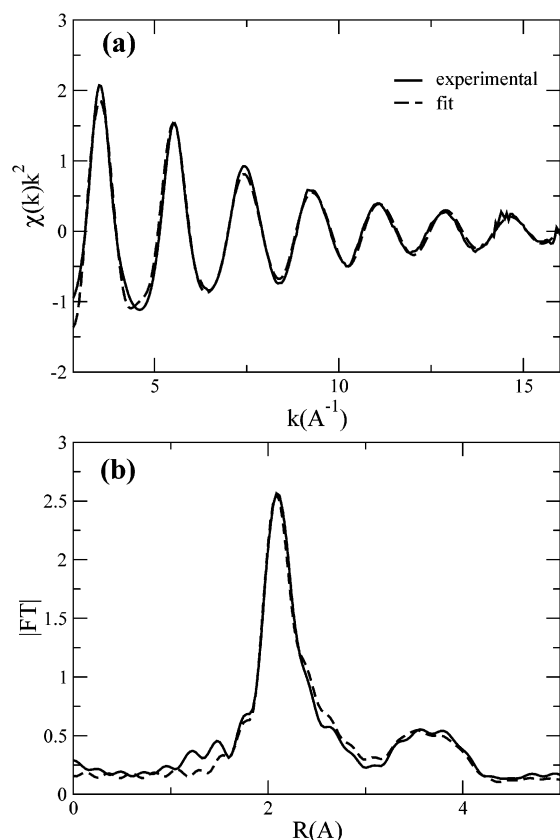
Figure 3. (a) L_{III}-edge EXAFS data, k^2-weighted, of the Ir(III) aqua ion in water: experimental function for the 0.33 M aqueous solution and fit obtained by using the parameters included in Table 1. (b) Amplitudes of their corresponding phase-corrected Fourier fransform.

Pd^{2+},[26b,54−59] it can be seen that the amplitude decreases more slowly than in these cases. Since the coordination number is the same in all cases, the slowest damping of the EXAFS signals points to a lower DW factor due to a small disorder in the Ir-(III) environment, which should be attributed to a higher kinetic stability.[9,28b]

Two model structures were considered to fit the EXAFS signal of the 0.33 M solution. In the first one, the central cation was surrounded by the six water molecules, forming the first hydration sphere. This implies a single scattering path, M−O_I (ss1 in Scheme 1), and the MS ones related with it (types A−D in Scheme 1). In the second model structure, in addition to the first hydration shell, a second one formed by 12 water molecules, located at a distance approximately double that of the first shell, was included. This implies two SS contributions, M−O_I and M−O_{II}, and the MS ones, A−D related with M−O_I. In both models coordination numbers were fixed, so that amplitudes were only dependent on DW factors. In the one/two shell fits 4/6 free parameters were used: coordination distances and DW factors for the first/and second shell, inner potential correction, ΔE_0, and amplitude reduction factor, S_0^2. Both model structures yield a rather good fit although that of the two shell model is slightly better. The best reproduction of the spectrum was obtained with the parameters included in Table 2. For comparative purposes, the corresponding values derived from the MD simulations have been included. It should be pointed out that the $\langle R \rangle$ values correspond to the mean distance (or expected distance) for the first and second peak in the Ir−O RDF. Figure 3 includes comparative plots of the two shells fit and experimental spectra of the $[Ir(H_2O)_6]^{3+}$complex. As seen there, a wide
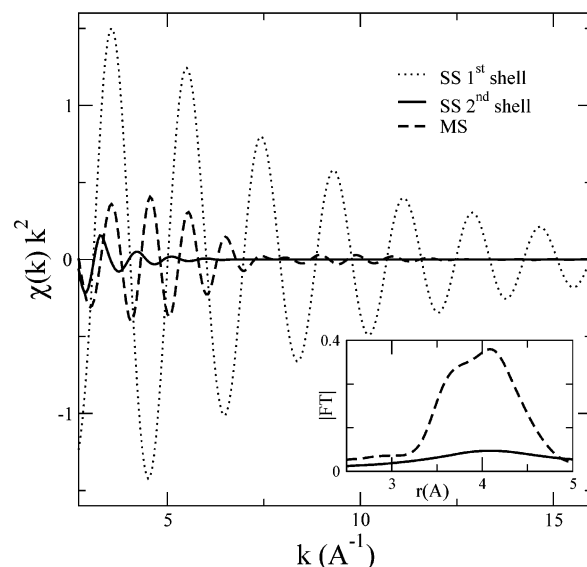

Figure 4. Contributions to the k-space EXAFS spectrum of the single scattering (SS) due to the first shell and second shell and the multiple scattering (MS) of the first shell. Inset shows the contribution to the second peak of the Fourier transform of the first-shell MS and the second-shell SS.

range of k (2.8−16 $Å^{-1}$) has been analyzed due to the excellent signal-to-noise ratio experimentally achieved.

Concerning the first shell, since there are no previous experimental results for the Ir−O coordination distance in solution, the value obtained here, 2.04 Å, is the first estimate of this bond distance. This value is similar to those previously obtained with XRD for some compounds in solid phase with a chemical structure close to that of the hexahydrate, i.e., *trans*-$[Ir(H_2O)_4Cl_2]^+$, with an Ir−O distance value[23] of 2.04 Å, and for the crystal structure of its the cesium alum above cited where the $[Ir(H_2O)_6]^{3+}$ motif presents a Ir−O distance of 2.041 Å.[25] There are no previous values for the DW factor of this shell either. Nevertheless, the value obtained here, 0.002 $Å^2$ is slightly smaller than that found for other trivalent transition metal cations,[26,27] as expected for its higher kinetic stability.

Although the first shell, including both SS and MS paths, is the main contribution to the spectrum, the fit improves slightly when a second coordination shell is included. As already observed in work with $[Cr(H_2O)_6]^{3+}$and $[Rh(H_2O)_6]^{3+}$ the detection of the second shell with XAS has a double problem: its intrinsic lability and the fact that its coordination distance is roughly twice that of the first shell. The first effect weakens the signal and renders its amplitude rather small as compared to that of the first shell. Due to the second effect, the frequency of this contribution overlaps with that of multiple scattering contributions within the first shell, as we have already shown.[26] Ir(III) cation presents an additional problem when compared with $[Cr(H_2O)_6]^{3+}$ and $[Rh(H_2O)_6]^{3+}$. Since it is heavier, the backscattering amplitude of the paths including Ir as an intermediate step becomes higher than the ones not including it. As a consequence, MS within the first shell becomes relatively more intense than the second-shell SS contribution. To show this more clearly, comparative plots of the EXAFS signal (in k space) defined by MS paths A−D versus that of the SS second shell for the iridium case have been included in Figure 4. The inset in this figure shows that the amplitude of the SS second shell is roughly one-fifth of that of MS first shell. In contrast, in Cr the amplitudes of both types of contributions were similar, while in Rh the amplitude of the second shell SS was about one-half that of the first shell MS (Figure 5 in ref
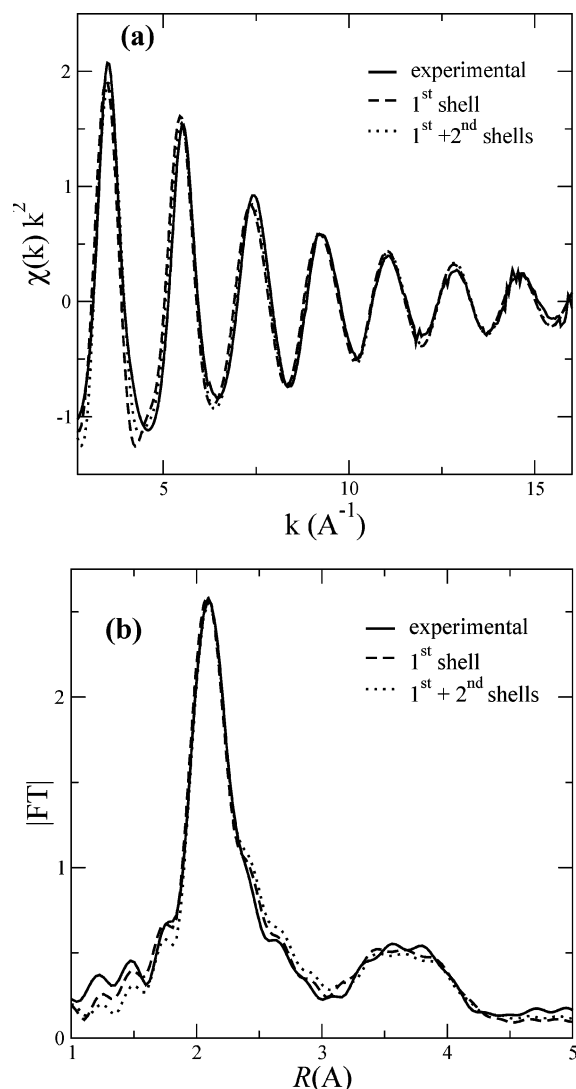
Figure 5. (a) Ir L_{III}-edge EXAFS spectra for aqueous $[Ir(H_2O)_6]^{3+}$ (0.33 M) and simulated spectra from a set of snapshots including only the first shell ($R_{cutoff} = 3.1$ Å) or beyond the second shell ($R_{cutoff} = 6.0$ Å) and (b) their amplitudes of their phase-corrected Fourier transform.

molecules or shells, by including them or not in the computation of the spectrum.

Figure 5a shows comparative plots of experimental EXAFS function and the simulated EXAFS function when either the first hydration shell only or a sphere including the two closest hydration shells are taken into account. Figure 5b compares their corresponding amplitudes of the phase-corrected Fourier Transform. The agreement among the experimental and both simulated spectra is satisfactory, as already observed in the conventional fit of the EXAFS spectrum. The first interesting conclusion is that the simulated spectrum using only the first hydration shell agrees fairly well with the experimental spectrum, the second hydration shell being only a marginal contribution to the EXAFS spectrum.

To test the reliability of the fitting procedure when such small contribution to the EXAFS function is involved in the data analysis, we have carried out the fitting of the simulated EXAFS spectra shown in Figure 5a, carrying out a conventional data analysis. Due to the correlation between the structural parameters, the coordination number for the second hydration shell has not been fitted, but several fixed values have been considered. The inclusion of the second shell improves only slightly the global fitting, the coordination distance, $R(Ir-O_{II})$ = 4.1 ± 0.1 Å, being quite independent of the coordination number (N_{II}), which is strongly coupled with the associated Debye–Waller factor, $\sigma^2(Ir-O_{II})$. This can be easily understood if the second peak in the Ir–O RDF is examined (Figure 1). In this figure, the integration number for this peak up to ca. 6.0 Å is close to 30 oxygen atoms; however within this broad peak, several types of oxygen atoms may be found. A set of 12–15 oxygen atoms belong to the water molecules that are strongly coordinated to the first-shell water molecules by hydrogen bonding, whereas the rest of them are rather bridge water molecules and are retained in the shell by less specific intermolecular interactions. When the number of oxygen atoms considered to contribute to the second shell SS of the EXAFS signal is larger, the global disorder associated with this shell becomes larger. It should be concluded that the determination of the second shell for Ir(III) from EXAFS function is rather difficult if there is no additional information to provide an estimation of some of the structural parameters associated to the global fitting. Once this is provided, the fitting results could be envisaged as an experimental confirmation of the second hydration shell.

A second interesting point is related with the EXAFS spectrum slightly below 5 Å^{-1}. The first minimum of the EXAFS oscillation shows the most significant discrepancy between experimental and computed spectra (Figure 5a). Interestingly, coming back to Figure 3a, where the experimental and fitted signals are plotted, the same discrepancy can be observed. The feature appearing at low k values is mainly due to multiple scattering contributions partially damped by the second hydration shell, as derived from the analysis of the corresponding simulated $\chi(k)k^2$ functions in Figure 5a. There are two possible reasons for this discrepancy. One is a partial failure of the simulated spectra. The other is the inaccuracy in the experimental signal due to the difficulty to extract this contribution of the raw data in the low-k region close to the intense L_{III}-edge white line. This second possibility has been explored by extracting the EXAFS function from the L_I-edge spectrum where there is not an intense white line. It was observed a nonsimple behavior of the oscillation in this part of the spectrum, similar to that observed in the simulated spectra. It has to be remembered that EXAFS of the L_{III}-edge is the one usually analyzed because it shows the higher intensity among L-edges and then the best signal/noise ratio. For this reason only the XANES part of the XAS spectra was recorded for L_I,
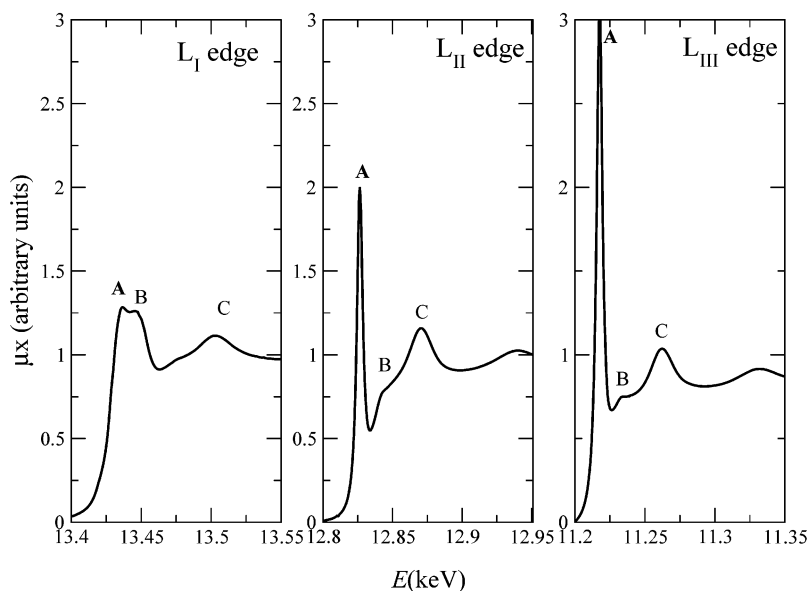
26c). Thus, the second hydration shell, that is expected to be the best defined in $[Ir(H_2O)_6]^{3+}$, because of its kinetic stability, turns out to be the most difficult to be detected by EXAFS due to this spectroscopic effect. In fact, it is a marginal contribution to the spectrum, and although the fit improves when taking into account this contribution, there is a high uncertainty in the parameters associated to this shell. In contrast, the parameters of the first hydration shell are not affected by its inclusion. Summarizing, from the EXAFS analysis highly accurate parameters are obtained for the first shell, while the second shell cannot be reliably detected due to spectroscopic effects.

Ir L_{III}-Edge EXAFS Spectrum Simulated from MD Snapshots. In an additional effort to gain information about the second shell structure, we have used additional sources of information, i.e., the structure and dynamics obtained from MD simulations. As explained in the subsection "EXAFS Spectrum Computations" of the Experimental Section, MD snapshots were used as input structures to compute a set of individual EXAFS spectra (in practice 1000 spectra were generated) by using eq 1 given in ther "EXAFS Spectrum Computations" subsection, where the individual EXAFS spectra are averaged and the simulated EXAFS spectrum is obtained. Within this procedure, since the structure associated to every snapshot is known, one may consider the influence on the spectrum of different atoms,

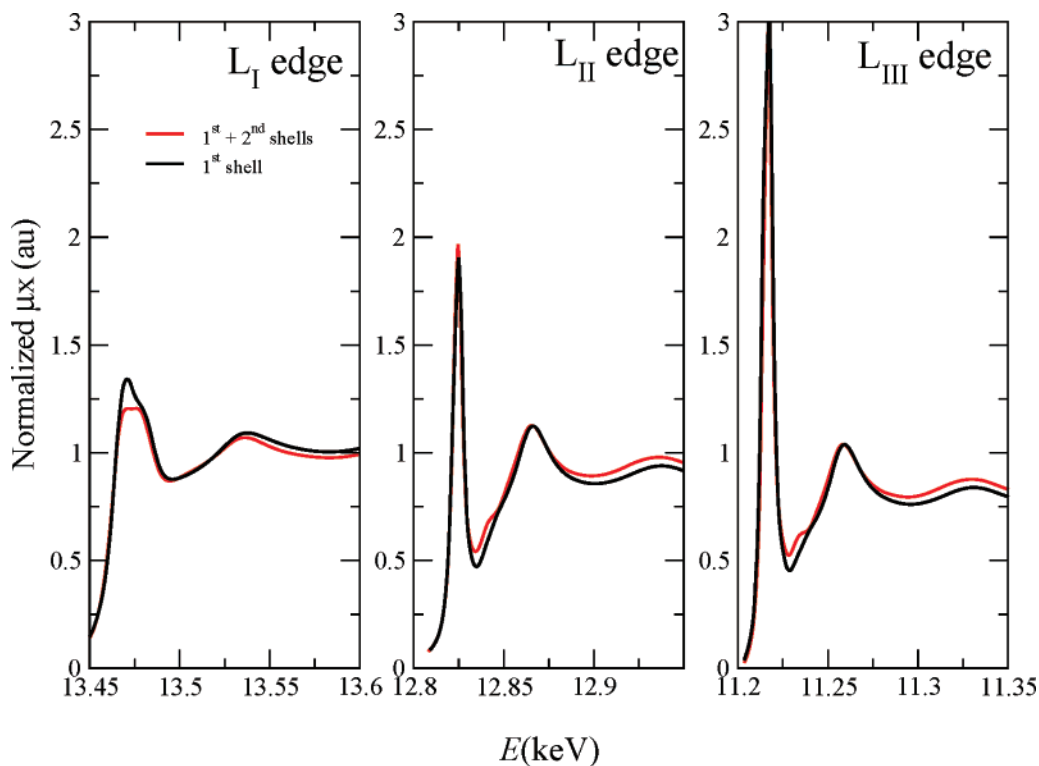**Figure 6.** Ir L-edges XANES experimental spectra for the 0.33 M $[Ir(H_2O)_6]^{3+}$ aqueous solution.

Figure 7. MD simulated Ir L-edges XANES spectra for $[Ir(H_2O)_6]^{3+}$ using a set of snapshots including only the first hydration shell ($R_{cutoff} = 3.1$ Å) (black) or beyond the second hydration shell ($R_{cutoff} = 6.0$ Å) (red).

so that a region of 200 eV above the edge was available for this additional analysis.

L-Edges Ir XANES Spectra of Aqueous [Ir(H₂O)₆]³⁺. Figure 6 shows the XANES region of the three L-edges of the experimental spectrum from aqueous solutions of $[Ir(H_2O)_6]^{3+}$. L edges correspond to transitions from the inner *l* level, atomic quantum number $n = 2$. L_{III} and L_{II}-edges, appearing at lower energy, are the transitions from 2p atomic levels while L_I-edge corresponds to transitions from *2s* level. L_{II} and L_{III}-edge shapes are obscured by the intense white line appearing just on top of the edge (labeled A) corresponding to transitions from *2p* to partially empty *nd* states. L_I edge has a different shape, being more similar to that of the K-edges which corresponds to a different transition. According to the general shape, L_{II} and L_{III} edges are similar, showing a sharp main peak, the so-called

white line, followed by a hump, labeled B, appearing 16 eV (for L_{III}) and 17 eV (for L_{II}) above the main resonance, with relative intensities of 5:1 (for L_{III}) and 3:1 (for L_{II}). The second broad peak, feature C, appears ca. 44 eV above the white line for both edges, but with different relative intensities, 3:1 and 2:1, for L_{III} and L_{II}, respectively. In contrast with the previous edges, the L_I presents a wide main resonance split in two small peaks 9 eV apart. A wide second peak appears 44 eV above the first peak of the main resonance similar to that observed in L_{II} and L_{III} edges. The ratio between the intensities of these two peaks is small, 1.2:1.

Figure 7 shows the computed spectra using two different cut-off radii, 3.1 and 6.0 Å for the structure considered for each snapshot. For both cut-off radii, a remarkable agreement between
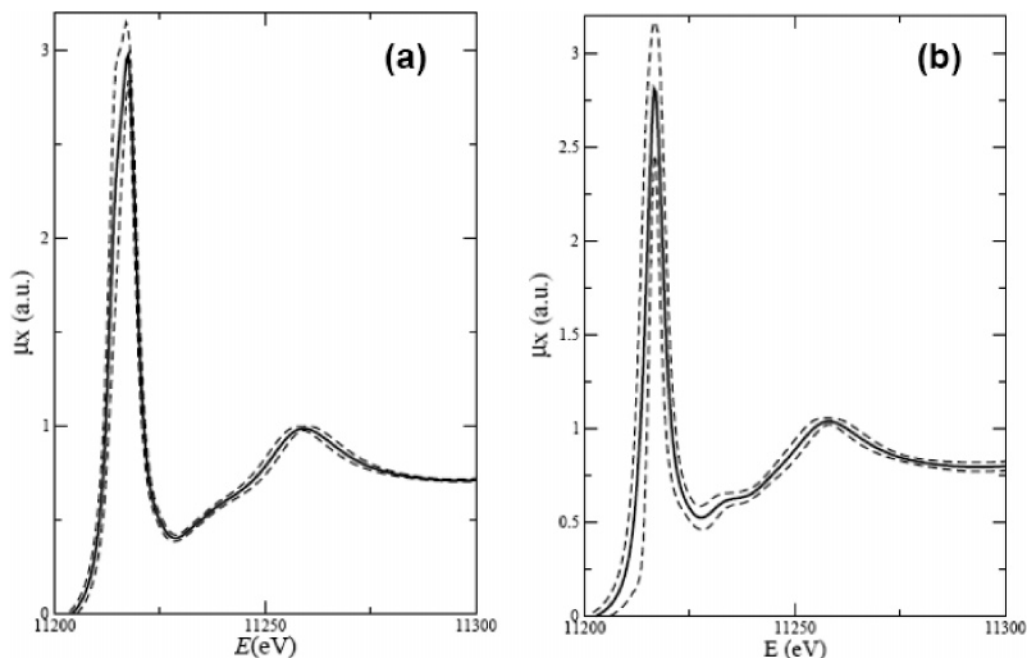
Figure 8. Calculated L$_{III}$-edge XANES spectra for [Ir(H$_2$O)$_6$]$^{3+}$: average spectrum (solid line) and its standard deviation (dashed line), considering only the first hydration shell (a) or beyond the second shell (b).

the experimental and theoretical spectra is achieved in the three edges, given that both the relative position of the peaks and the shape of the curves are well reproduced by simulated spectra. This is a clear indication that the two theoretical tools employed for the generation of the XANES spectrum supply an accurate description of the spectroscopic properties: the MD simulation and, thus implicitly, the intermolecular potentials employed as well as the ab initio FEFF8.10 code used to compute the XAS spectra. This rather good agreement between computed and experimental spectra, together with the reasonable values of other nonspectroscopic properties, presented in the MD simulation results section, gives a strong support to the reliability of the intermolecular interaction potentials developed for the iridium cation. Likewise, it is an additional support to the reliability of the predicted values found for the nonstructural properties obtained from the simulation which have not been experimentally determined yet. Moreover, the absolute position of the computed spectrum is only 3 eV off from the experimental one for the case of the L$_{II}$ and L$_{III}$ edges, whereas in the case of the L$_I$ this shift is ca. 40 eV. These values represent relative shifts of 0.03% and 0.3% of the total edge energy for L$_{II}$ and L$_{III}$, and L$_I$, respectively, which are a rather accurate estimation of the absolute energy of the Fermi level by quantum mechanisms, bearing in mind the increasing difficulties when heavy atoms and inner levels are involved in the ionization process.[35] Given these theoretical difficulties some computing codes work with relative values[60,61]

The main discrepancy of the experimental XANES spectra with those computed from the structure including only the first hydration shell (R_{cutoff} = 3.1 Å, dashed lines in Figure 7) is the lack of the hump B for L$_{II}$- and L$_{III}$-edges, and the lack of the split in the main edge resonance in the L$_I$-edge spectrum. The inclusion of the second hydration shell in the structure used to compute the theoretical spectra leads to the appearance of the previous missing features, that is, feature B in the L$_{II}$- and L$_{III}$-edges and the increase of the relative intensity of the second peak in the main resonance, thus giving rise to the splitting of the main resonance. These structural relationships found for the three L-edges in the case of aqueous solutions have its

equivalence in the previous cases studied for the K-edge of Cr and Rh[28] and the L$_{III}$-edge of Pt,[54] where it was observed how the effect of the second hydration shell on the general shape of their corresponding XANES spectra was an increase of the relative intensity for humps just 10−15 eV above the main resonance.[28b] As this feature appears to be associated with the second hydration shell for several cations and different edges,[28,54] it seems reasonable to accept that it could be considered a general spectroscopic behavior. To confirm such hypothesis, a careful and systematic examination along a wide series of XANES spectra of transition metal ions in aqueous solution should be carried out.

The results for [Ir(H$_2$O)$_6$]$^{3+}$ presented here are particularly relevant in two aspects. First, as shown above, the same geometrical structures produces three different XANES spectra, those from L$_I$-, L$_{II}$-, and L$_{III}$-edges. Then the simulations of three spectra and the observation that the second hydration shell improves in a non-negligible way the reproduction of each edge reinforce the confidence in the conclusions of the study. Second, contrary to the case of other trivalent cations, it was rather difficult to determine unambiguously the second hydration shell by analyzing the EXAFS spectrum. Then, for [Ir(H$_2$O)$_6$]$^{3+}$ the evidence of a well-defined second hydration shell rests mainly on the XANES spectrum. More recently, D'Angelo et al.[29] following a similar strategy to compute the XANES spectra, have reached similar conclusions regarding the possibility of assigning the second hydration shell of [Ni(H$_2$O)$_6$]$^{2+}$ on the basis of the XANES spectrum features.

The microscopic description of the system supplied by the MD simulations has allowed us a further analysis of the fluctuations in the structure. More specifically it enabled the computation of an average spectrum obtained from the contribution of 200 individual spectra based on 200 different structures visited by the system during its trajectory along the configurational space. By analyzing this trajectory, it was possible to determine the standard deviation associated with each point of the averaged spectrum.

Figure 8 represents the computed spectra obtained when only the first hydration shell was considered in the snapshot (Figure

8a) or when the two first shells were included (Figure 8b). The average spectrum appear drawn with solid lines, which are enclosed by two dashed lines giving twice the standard deviation, so 95% of the spectra contributing to the averaged one is included in the range defined. The narrower corridor appearing in the case of the first-shell hydration structure points out that the second hydration shell is not only modifying some features of the spectrum but also adding significant fluctuations to the final form. At the electronic level a wider fluctuation is observed as well for the two-shell model, observed by examining the average value for the Fermi level obtained for the same set of XANES computations. When only the first shell is taken into account, the Fermi level energy is 11 220 ± 0.06 eV, while considering two hydration shells it is 11 225 ± 0.6 eV. These figures indicate that there are two significant factors associated with the hydration of the aqua ion. The first is the implicit dielectric behavior of the outer water shells, which stabilize the electropositive character of the aqua ion and as a consequence the ionization energy increases. The second factor is the increase of the fluctuations with the number of molecules interacting and the weakness of the intermolecular interactions of outer shells with respect to the strong direct interaction among the central cation and its first-shell water molecules.

Therefore, this general behavior suggests that strategies associated with the determination of structural parameters from a XANES spectrum would become more difficult when the number of shells taken into account in the computation increases. The geometrical fluctuations become larger, and thus the concept of the pattern to be fitted becomes more diffuse. Techniques accounting for these fluctuations which could include this fluxional behavior in some way certainly would help in the structural resolution procedures.

Concluding Remarks

The Ir−O distance corresponding to the first hydration shell of Ir(III) in aqueous solution has been determined independently from EXAFS spectroscopy and MD simulations based on a new first-principles intermolecular potential for Ir−water. The value obtained with both techniques is the same, 2.04 ± 0.01 Å. MD Ir−O RDF shows that the second hydration shell is defined by a broad peak centered at 4.05 Å formed by 14−15 water molecules. On the contrary to what expected, the detection of the second hydration shell by EXAFS for Ir(III) is more difficult than for other less stable aqua ion such as Cr(III) and Rh(III).[26,28b] In fact, it is a marginal contribution to the spectrum, and although the fit improves when taking into account this contribution, there is a high uncertainty in the parameters associated to this shell.

In contrast with the diffuse manifestation of the second shell in the EXAFS spectrum, the XANES region corresponding to the three Ir L-edges shows well-defined features that can be clearly ascribed to the second hydration shell. This is proven when XANES spectra are simulated for the structural information derived from MD simulations with and without this shell. To our knowledge, this is the first time that three different edges of the same system are theoretically computed. They simultaneously and concurrently support a specific structural property, the presence of the second hydration shell around a stable trivalent metal cation in solution.

The advantage shown by XANES against EXAFS to detect a minor structural contribution, as the second hydration shell is, should be rationalized as a consequence of the dependence of the Debye−Waller factor with the vector k. The signal is damped in an exponential way with the increase of k, so the

structural disorder is less relevant for low k-values, i.e., in the XANES region. The key point is to provide a source of information XAS-independent, such as computer simulations, being able to relate features and structural properties of the systems under study.

MD simulation has provided additional non-structural information on the Ir(III) aqua ion in water. Self-diffusion coefficient at 298 K is $0.6 \pm 0.1 \times 10^{-5}$ cm^2 s^{-1}, hydration enthalpy is estimated at -5500 ± 160 kJ/mol, and the mean residence time for water molecules in the second hydration shell is in the range of 9−19 ps.

The statistical nature of the simulated XANES spectrum has allowed the evaluation of the standard deviation associated to the average spectrum as a function of the shells included in the simulation. The increase of the standard deviation with the number of shells included is the spectroscopic consequence of the larger fluctuations of the solvent structure at longer distance of the cation. This behavior is responsible of the smoothing of characteristic features associated to structural properties far away from the absorber atom.

We believe that this work is showing how the combination of experimental and theoretical analysis of the XAS spectra, when possible extended to the simultaneous study of several edges, is extremely useful to get deeper insights in the structural and dynamic behavior of metal ions in solution and illustrates a promising line of endeavor toward the similar investigation of many other hitherto unexplored examples.

Supporting Information Available: FFFF input file to generate the simulated EXAFS function from a snapshot of the MD simulation and FFFF input file ot generate the simulated XANES function from a smapshot of the MD simulation. This material is available free of charge via the Internet at http://pubs.acs.org.

References and Notes

(1) Burgess, J. *Ions in Solution*; Ellis Horwood: Chichester, U. K., 1986.

(2) Conway, B. E. *Ionic Hydration in Chemistry and Biophysics*; Studies in Physical and Theoretical Chemistry 12; Elsevier: Amsterdam, 1981.

(3) Barthel, J. M. G.; Krienke, H.; Kunz, W. *Physical Chemistry of Electrolyte Solutions*; Steinkopff: Darmstadt, The Netherlands, 1998.

(4) Marcus, Y. *Ion Solvation*; Wiley: Chichester, U. K., 1986.

(5) Magini, M.; Licheri, G.; Paschina, G.; Piccaluga, G.; Pinna, G. *X-ray Diffraction of Ions in Aqueous Solution: Hydration and Complex Formation*; CRC Press: Boca Raton, FL, 1988.

(6) Ohtaki, H.; Radnai, T. *Chem. Rev.* **1993**, *93*, 1157.

(7) Neilson, G. W.; Enderby, J. E. *J. Phys. Chem.* **1996**, *100*, 1317.

(8) Sayers, D. E.; Stern, E. A.; Lytle, F. W. *Phys. Rev. Lett.* **1971**, *27*, 1204.

(9) Miyanaga, T.; Sakane, H.; Watanabe, I. *J. Synchrotron Radiat.* **2001**, *8*, 680.

(10) Teo, B. K. *EXAFS: Basic Principles and Data Analysis*; Springer-Verlag: Berlin, 1986.

(11) Filipponi, A.; D'Angelo, P.; Pavel, N. V.; Di Cicco, A. *Chem. Phys. Lett.* **1994**, *225*, 150.

(12) Palmer, B. J.; Pfund, D. M.; Fulton, J. L. *J. Phys. Chem.* **1996**, *100*, 13393.

(13) Campbell, L.; Rehr, J. J.; Schenter, G. K.; McCarthy, M. I.; Dixon, D. *J. Synchrotron Radiat.* **1999**, *6*, 310.

(14) Jalilehvand, F.; Spångberg, D.; Lindqvist-Reis, P.; Hermansson, K.; Persson, I.; Sandström, M. *J. Am. Chem. Soc.* **2001**, *123*, 431.

(15) Merkling, P. J.; Muñoz-Páez, A.; Martínez, J. M.; Pappalardo, R. R.; Marcos, E. S. *Phys. Rev. B* **2001**, *64*, 012201.

(16) Glezakov, V. A.; Chen, Y. S.; Fulton, J. L.; Schenter, G. K.; Dang, L. X. *Theor. Chem. Acc.* **2006**, *115*, 86.

(17) (a) Hunt, J. P.; Taube, H. *J. Chem. Phys.* **1950**, *18*, 757. (b) Hunt, J. P.; Taube, H. *J. Chem. Phys.* **1951**, *19*, 602.

(18) (a) Stranks, D. R.; Swaddle, T. W. *J. Am. Chem. Soc.* **1971**, *93*, 2783. (b) Laurenczy, G.; Rapaport, I.; Zbinden, D.; Merbach, A. E. *Magn. Reson. Chem.* **1991**, *29*, S45.

(19) Beutler, P.; Gamsjäger, H. *J. Chem. Soc., Chem. Commun.* **1976**, 554.

(20) Beutler, P.; Gamsjäger, H.; Baertschi, P. *Chimia* **1978**, *5*, 163.

(21) Cusanelli, A.; Frey, U.; Richens, D. T.; Merbach, A. E. *J. Am. Chem. Soc.* **1996**, *118*, 5265.

(22) McMahon, M. R.; McKenzie, A.; Richens, D. T. *J. Chem. Soc., Dalton. Trans.* **1988**, 711.

(23) Richens, D. T. *The Chemistry of Aqua Ions*; Wiley: Chichester, U. K., 1997, Chapter 9.

(24) Frank, H. S.; Evans, M. W. *J. Chem. Phys.* **1945**, *13*, 507.

(25) Armstrong, R. S.; Beattie, J. K.; Best, S. P.; Skelton, B. W.; White, A. H. *J. Chem. Soc., Dalton Trans.* **1983**, 1973.

(26) (a) Muñoz-Páez, A.; Marcos, E. S. *J. Am. Chem. Soc.* **1992**, *114*, 6931. (b) Muñoz-Páez, A.; Pappalardo, R. R.; Marcos, E. S. *J. Am. Chem. Soc.* **1995**, *117*, 11710. (c) Sakane, H.; Muñoz-Páez, A.; Díaz-Moreno, S.; Martínez, J. M.; Pappalardo, R. R.; Marcos, E. S. *J. Am. Chem. Soc.* **1998**, *120*, 10397.

(27) Lindqvist-Reis, P.; Muñoz-Páez, A.; Díaz-Moreno, S.; Pattanaik, S.; Persson, I.; Sandström, M. *Inorg. Chem.* **1998**, *120*, 10397.

(28) (a) Merkling, P. J.; Muñoz-Páez, A.; Pappalardo, R. R.; Marcos, E. S. *Phys. Rev. B.* **2001**, *64*, 092201. (b) Merkling, P. J.; Muñoz-Páez, A.; Marcos, E. S. *J. Am. Chem. Soc.* **2002**, *124*, 10911.

(29) D'Angelo, P.; Roscioni, O. M.; Chillemi, G.; Della Longa, S.; Benfatto, M. *J. Am. Chem. Soc.* **2006**, *128*, 1853.

(30) Pappalardo, R. R.; Marcos, E. S. *J. Phys. Chem.* **1993**, *97*, 4500.

(31) Pappalardo, R. R.; Martínez, J. M.; Marcos, E. S. *J. Phys. Chem.* **1996**, *100*, 11748.

(32) Martínez, J. M.; Pappalardo, R. R.; Marcos, E. S. *J. Chem. Phys.* **1998**, *109*, 1445.

(33) Castillo-Blum, S. E.; Richens, D. T.; Sykes, A. G. *J. Chem. Soc., Chem. Commun.* **1986**, 1120.

(34) Yokoyoma, T.; Kobayashi, K.; Ohta, T.; Ugawa, A. *Phys. Rev. B* **1996**, *53*, 6111.

(35) Ankudinov, A.; Ravel, B.; Rehr, J. J.; Conradson, S. D. *Phys. Rev. B* **1998**, *58*, 7565.

(36) Stern, E. A.; Newville, M.; Ravel, B.; Yacoby, Y.; Haskel, D. *Physica B* **1995**, *208−209*, 117.

(37) Martínez, J. M.; Pappalardo, R. R.; Marcos, E. S. *J. Am. Chem. Soc.* **1999**, *121*, 3175.

(38) Martínez, J. M.; Merkling, P. J.; Pappalardo, R. R.; Refson, K.; Marcos, E. S. *Theor. Chem. Acc.* **2004**, *111*, 101.

(39) Martínez, J. M.; Torrico, F.; Pappalardo, R. R.; Marcos, E. S. *J. Phys. Chem. B* **2004**, *108*, 15851.

(40) Jorgensen, W. L.; Chandrasekhar, J.; Madura, J. D.; Impey, R. W.; Klein, M. D. *J. Chem. Phys.* **1983**, *79*, 926.

(41) Dolg, M.; Stoll, H.; Preuss, H.; Pitzer, R. M. *J. Chem. Phys.* **1993**, *97*, 5852. Modifications included at http://www.emsl.pnl.gov:2080/forms/basisform.html were also used.

(42) Woon, D.; Dunning, T. H., Jr. *J. Chem. Phys.* **1993**, *98*, 1358.

(43) (a) Miertus, S.; Scrocco, E.; Tomasi, J. *Chem. Phys.* **1981**, *55*, 117. (b) Mennucci, B.; Cancès, E.; Tomasi, J. *J. Phys. Chem. B* **1997**, *101*, 10506.

(44) Brenemam, C. M.; Wiber, K. B. *J. Comput. Chem.* **1990**, *11*, 361.

(45) (a) Nosé, S. *Mol. Phys.* **1984**, *52*, 255. (b) Hoover, W. G. *Phys. Rev. A* **1985**, *31*, 1695.

(46) Refson, K. *Comput. Phys. Commun.* **2000**, *126*, 310.

(47) Allen, M. P.; Tildesley, D. J. *Computer Simulations of Liquids*; Oxford University Press: Oxford, U. K., 1987; pp 155−162.

(48) Leslie, M.; Gillan, M. *J. Phys.: Condens. Matter* **1985**, *18*, 973.

(49) Roberts, J. E.; Schnitker, J. *J. Phys. Chem.* **1995**, *99*, 1322.

(50) Figuereido, F.; Del Buono, G. S.; Levy, R. M. *J. Chem. Phys.* **1995**, *103*, 6133.

(51) Bogusz, S.; Cheatham, T. E.; Brooks, B. R. *J. Chem. Phys.* **1998**, *108*, 7070.

(52) Merkling, P. J.; Muñoz-Páez, A.; Martínez, J. M.; Pappalardo, R. R.; Marcos, E. S. *Phys. Rev. B* **2001**, *64*, 012201.

(53) Mink, J.; Németh, C.; Hajba, L.; Sandström, M.; Goggin, P. L. *J. Mol. Struct.* **2003**, *661−662*, 141.

(54) Ayala, R.; Marcos, E. S.; Díaz-Moreno, S.; Solé, V. A.; Muñoz-Páez, A. *J. Phys. Chem. B* **2001**, *105*, 7588.

(55) Hellquist, B.; Bengtsson, L. A.; Holmberg, B.; Hedman, B.; Persson, I.; Elding, L. I. *Acta Chem. Scand.* **1991**, *45*, 449.

(56) D'Angelo, P.; Barone, V.; Chillemi, G.; Sanna, N.; Meyer-Klaucke, W.; Pavel, N. V. *J. Am. Chem. Soc.* **2002**, *124*, 1958.

(57) Fulton, J. L.; Heald, S. M.; Badyal, Y. S.; Simonson, J. M. *J. Phys. Chem. A* **2003**, *107*, 4688.

(58) Purans, J.; Fourest, B.; Cannes, C.; Sladkov, V.; David, F.; Venault, L.; Lecomte, M. *J. Phys. Chem. B* **2005**, *109*, 11074.

(59) Carrera, F. Estudio de la Estructura en Disolución de Complejos de Elementos de Transición Relacionados con Sistemas de Interés Biológico Mediante Espectroscopía de Absorción de Rayos X. Ph.D. Thesis. Universidad de Sevilla, Sevilla, Spain, 2005.

(60) Tyson, T. A.; Hodgson, K. A.; Natoli, C. R.; Benfatto, M. *Phys. Rev. B* **1992**, *46*, 5997.

(61) Bugaev, L. A.; Ildefonse, P.; Flank, A.-M.; Sokolenko, A. P.; Dmitrienko, H. V. *J. Phys.: Condens. Matter* **1998**, *10*, 5463.